Published in final edited form as:
Invest Ophthalmol Vis Sci. 2009 August ; 50(8): 3542–3552. doi:10.1167/iovs.09-3460.

TGFBIp inhibits the attachment of human scleral fibroblasts to collagen type I

Lilian Shelton and **Jody Summers Rada, Ph.D.**
Department of Cell Biology, University of Oklahoma Health Science Center, Oklahoma City, Oklahoma

Abstract

Purpose—Transforming growth factor beta-induced protein, 68kD (TGFBIp) is a secreted extracellular matrix (ECM) protein that has been demonstrated to regulate cell attachment in a variety of cell types. The sclera synthesizes and secretes TGFBIp, which may function to facilitate scleral ECM remodeling events associated with myopia development. Here we report *TGFBI* expression by human scleral fibroblasts (HSFs), and that its protein product, TGFBIp, mediates an effect on cell attachment.

Methods—*TGFBI*/TGFBIp expression was evaluated by RT-PCR and immunoblot of HSF lysates and culture supernatants. The effect of rTGFBIp (50 μg/ml) on cell attachment to collagen-type I was determined using fluid phase cell attachment assays in HSFs, human foreskin fibroblasts (HFFs) and human corneal stroma fibroblasts (HCFs). Binding assays using biotinylated rTGFBIp were used to assess TGFBIp binding to the HSF surface. Flow cytometry and immunocytochemistry were used to determine both αvβ3 and αvβ5 expression, and localization to the HSF cell surface.

Results—HSFs express *TGFBI* and secrete TGFBIp (~833 ng/hr). rTGFBIp significantly decreased (25 μg/ml, $p \leq 0.05$) HSF attachment to collagen-type I, whereas rTGFBIp did not significantly effect cell attachment of HFFs ($p = 0.50$) or HCFs ($p = 0.24$) to collagen, as compared with BSA. Integrins αvβ3 and αvβ5 were detected on the cell surface, and both anti-αvβ3 and anti-αvβ5 functionally blocked rTGFBIp binding to HSFs.

Conclusions—TGFBIp plays an inhibitory role of HSF attachment to collagen type I, in vitro, through interactions with both αvβ3 and αvβ5 integrin receptors. These results suggest that TGFBIp may modulate scleral cell-matrix interactions, in vivo, thereby affecting scleral viscoelasticity.

Keywords

human scleral fibroblasts; cell adhesion; TGFBIp; BIGH3; keratoepithelin; integrin

Introduction

The mammalian sclera provides structural support for the delicate inner ocular tissues and defines the size, shape and refractive status of the eye. The sclera is a dense connective tissue consisting largely of extracellular matrix (ECM) containing collagen types I and III (Zorn N, et al. *IOVS* 1992;33:ARVO Abstract S1053; Norton TT and Miller EJ. *IOVS* 1995;36: ARVO Abstract S760)[1-3] as well as lesser amounts of collagens IV, V, VI, VIII, XII and XIII (Zorn N, et al. *IOVS* 1992;33:ARVO Abstract S1053; Norton TT and Miller EJ. *IOVS* 1995;36: ARVO Abstract S760),[1-7] proteoglycans (Johnson JM, et al. *IOVS* 2002;43:ARVO E-Abstract

Corresponding Author: Jody Summers Rada, Ph.D., Department of Cell Biology, University of Oklahoma Health Sciences Center, 940 Stanton L. Young Blvd., Oklahoma City, Oklahoma, 73104, jody-summersrada@ouhsc.edu, Phone: (405)271-3486, Fax: (405)271-3548.

1100)[8-12] and noncollagenous glycoproteins.[13-14] The scleral ECM is organized into irregularly arranged collagenous lamellae which are continuous with the highly ordered collagenous lamellae of the cornea at the corneal limbus. Located between the collagenous lamellae of the sclera are scleral fibroblasts that are responsible for the synthesis and turnover of the scleral ECM.[15]

Myopia is a common abnormal visual condition characterized by a negative refractive error that occurs when the eye is too long for its focal length. In humans, this ocular elongation is associated with significant scleral thinning and alterations in collagen fibril density and morphology at the posterior pole of the eye.[16-18] Mammalian models of myopia have also demonstrated scleral thinning as well as changes in gene expression and protein synthesis during the development of myopia.[15,19-26] More specifically, myopia development in mammals is associated with a decreased rate of proteoglycan synthesis,[20,24,27-28] decreased collagen fibril diameter and synthesis,[3,18,21,29] and increased matrix metalloproteinase-2 (MMP-2) activity.[21,30-32] Although the events leading to myopia development are not clear, these biochemical changes in the scleral extracellular matrix have been associated with alterations in the biomechanical properties of the sclera and are thought to be responsible for the increased rate of ocular elongation and development of myopia.[33-35]

Of much interest are the molecular mechanisms which regulate scleral cell-matrix interactions under normal ocular growth conditions as well as under conditions of increased ocular elongation and myopia development. Observations in animal models strongly suggest that local factors within the eye play an important role in the regulation of ocular growth.[19,36-40] Furthermore, scleral proteoglycan synthesis has been shown to be regulated in part, by the involvement of the underlying vascular layer of the eye, the choroid.[41-43] These studies suggest that the eye is not dependent on the brain for visually guided growth regulation, but rather is dependent on a cascade of chemical events extending from the retina to the sclera act to control vitreous chamber elongation.

Recently, microarray analyses were used to identify genes differentially expressed in choroid/RPEs in eyes of young marmosets (*Callithrix jacchus*) during varying ocular growth states.[44] The transforming growth factor beta-inducible gene-h3 (*TGFBI*; also known as *BIGH3*, *βIGH3*) was shown to be significantly increased in the choroid/RPE of eyes compensating for -5 D lenses (relative myopia) as compared with contralateral +5 D lens-treated eyes (relative hyperopia). Additionally, expression of the *TGFBI* gene product, TGFBIp (also known as BIGH3, βIG-H3 and keratoepithelin),[45-46] was identified in both the marmoset and human cornea, choroid/RPE, and was also present in high levels in the sclera.[44]

To date, several studies have suggested that TGFBIp plays a functional role in cell adhesion, migration, proliferation, wound healing, inflammation, tumorigenesis, angiogenesis, nephropathies and corneal dystrophy.[47] Until now, *TGFBI*/TGFBIp expression and its possible functional role(s) in the sclera have not been studied. Therefore in the present study, in vitro analyses using primary human scleral fibroblasts (HSFs) were undertaken to evaluate the scleral expression of *TGFBI*/TGFBIp and determine its role in mediating scleral fibroblast attachment to collagen-type I. The results of these studies demonstrate that TGFBIp selectively and specifically inhibits attachment of HSFs to collagen-type I, most likely through interactions with αvβ3 and αvβ5 integrin receptors located on the HSF cell surface. These results may provide insights into the role of TGFBIp in scleral remodeling events required for normal ocular growth as well as during the development of myopia.

Methods

Cell culture

Primary human scleral fibroblasts (HSFs) were isolated from explants of human donor sclera as previously described and stored in liquid nitrogen until use.[48-49] Primary human corneal fibroblasts (HCFs) were isolated from stromal explants from the central regions of human donor corneas as previously described and stored in liquid nitrogen until use.[50] HSFs, passages 4 – 6 (P_{4-6}), and HCFs (P_{6-9}) were cultured on 100 mm plates containing Dulbecco's modified Eagle's medium (DMEM), penicillin (100 units/ml)-streptomycin (100 μg/ml) and amphotericin B (0.0025 μg/ml) (1× a/a; Invitrogen Corp., Carlsbad, CA) and 15% fetal bovine serum (FBS) at 37 °C with 95% air/5% CO_2. Human foreskin fibroblasts (HFFs, P_{3-6}) were obtained from American Type Culture Collection (ATCC, Manassas, VA) and cultured in Iscove's modified Eagle's medium (IMEM) (ATCC, Manassas, VA) containing 1× a/a and 10% FBS at 37 °C with 95% air/5% CO_2 HSF conditioned medium was obtained from confluent cultures by replacing the culture media with serum-limiting media (DMEM containing 1× a/a and 0.05 % FBS) and incubating for 48 hrs at 37 °C in 95% air/5% CO_2. For cell attachment assays (see below) culture media was removed from confluent cultures and cells were rinsed once and then incubated in 0.53 mM EDTA in Hank's balanced salt solution (HBSS) (Sigma-Aldrich, St. Louis, MO) at 37 °C for 10 min. Following incubation in 0.53 mM EDTA, cells were detached by gentle pipeting, centrifuged and resuspended in DMEM containing 1× a/a prior to counting with a hemocytometer.

RNA isolation and cell lysate preparation

Following the 48 hr incubation, the conditioned media was collected, and either RNA was isolated or cell lysates were obtained from the HSF cell layers. Total RNA was isolated from HSF monolayers using TRIZOL Reagent following the standard protocol (Invitrogen Corp., Carlsbad, CA) as previously described.[44] Isolation of whole cell extracts was performed using a commercial mammalian cell lysis buffer, M-PER (Pierce Chemical, Rockville, IL), protease inhibitor cocktail set 1 (EMD Biosciences, San Diego, CA), phosphatase inhibitor cocktail 2 (Sigma Chemical, St. Louis, MO) and NaCl. The protease inhibitor cocktail set 1 contains five protease inhibitors that inhibits a broad range of proteases (500 μM 4-(2-aminoethyl) benzenesulfonylfluoride-hydrochloride, 150 nM aprotinin, 1 μM E-64 protease inhibitor, 0.5 mM EDTA-disodium, 1 μM leupeptin-hemisulfate) and the phosphatase inhibitor cocktail 2 contains a proprietary mixture of inhibitors that inhibits acid and alkaline phosphatases as well as tyrosine protein phosphatases (sodium orthovanadate, sodium molybdate, sodium tartrate, imidazole). The lysis buffer was prepared by diluting protease inhibitor cocktail set 1 (1:100) and phosphatase inhibitor cocktail set 2 (1:100) in M-PER (4.6 ml) containing 150 mM NaCl. Briefly, the cells were washed with ice-cold PBS for 1 min before the addition of lysis buffer (200 μl/plate), then scraped with a rubber policeman and collected. Following incubation (15 min) on ice and centrifugation (12,000 × g) for 5 min, the supernatant was collected and stored at -20 °C until use.

RT-PCR

cDNA was synthesized from total RNA using MuLV reverse transcriptase together with random hexamers, dNTPs in the presence of PCR buffer, 25 mM $MgCl_2$, and RNase inhibitor (GeneAmp kit; Applied Biosystems, Foster City, CA) as previously described.[44,48] Primers specific for human *TGFBI* and cyclophilin A [peptidylprolyl isomerase A (*PPIA*)], were designed and purchased using BLAST, Primer3 (http://frodo.wi.mit.edu/cgi-bin/primer3/primer3_www.cgi) and Sigma-Genosys (St. Louis, MO), respectively, and diluted to 15 μM in RNase-free water as previously described.[44] Cyclophilin A served as a positive control in this study as it has been routinely used as a housekeeping gene to normalize for gene expression differences, and has previously been

shown to consistently generate high quality PCR products with a high efficiency, while showing no significant differences in steady-state mRNA levels in the choroid/RPE of minus lens-treated eyes (undergoing relative myopia development) as compared with that of plus lens-treated eyes (undergoing relative hyperopia development) in marmosets.[44]

Each reaction underwent 35 amplification cycles consisting of denaturation at 94 °C for 30 sec, annealing for 30 sec at 60 °C, and extension for 30 sec at 72 °C using a DNA thermal cycler 480 (Perkin Elmer, Norwalk, CT). To control for genomic DNA contamination, reverse transcriptase was omitted from some samples prior to PCR amplification. Aliquots of each PCR reaction were electrophoresed on a 1.5% agarose gel containing ethidium bromide (0.5 μg/ml) and visualized on a Chemigenius imager (Syngene USA, Frederick, MD).

Western blot analysis

Following the 48 hr of incubation in DMEM + 0.05% FBS, conditioned medium was collected from HSF cell cultures, and cell lysates were dried under a vacuum in a Speed-Vac concentrator (Savant, Holbrook, NY) and reconstituted in 1/10 of the original volume with RNase-free water to concentrate the intracellular TGFBIp protein. Scleral cell lysates and aliquots of conditioned medium were directly applied to 10% Bis-Tris Gel NuPAGE™ SDS-PAGE gels (Invitrogen Corp., Carlsbad, CA). Gel samples were electrophoresed under reducing conditions and electroblotted onto a nitrocellulose membrane using an electro-transfer unit (XCELL Sureback™ Electrophoresis Cell, Invtirogen, Carlsbad, CA) according to manufacturer's instructions. Blots were blocked with PBS containing 0.1% Tween-20 and 0.2% I-Block (Tropix, Bedford, MA) for 1 hr then probed with anti-human TGFBIp (1:500, R&D Systems, Minneapolis, MN) or mouse monoclonal α-tubulin (1:10000, Abcam, Cambridge, MA) antibodies overnight at 4 °C. Anti-human TGFBIp is a polyclonal antibody that was produced in goats immunized with purified, NS0-derived (mouse myeloma cell line), mature recombinant human TGFBIp protein (Gly 24-His 683).[45] The specific epitope(s) this antibody recognizes has not been characterized, but has been used in a previous study to recognize a 68 kD band in primate ocular tissues.[44] Immunoblots were then washed three times for 10 min with PBS containing 0.05% Tween-20 and incubated with rabbit anti-goat IgG (whole molecule) conjugated to alkaline phosphatase or goat anti-mouse IgG (whole molecule) conjugated to alkaline phosphatase secondary antibodies (1:1000, Sigma, St. Louis, MO) for 1 hr at room temperature. Following incubation with secondary antibody, blots were washed, incubated with CDP-*Star* ® Ready-to-Use with Nitro-BlockII™ (Tropix, Bedford, MA) for 5 min and then imaged with a Chemigenius imager (Syngene USA, Frederick, MD) or exposed to film. In some cases, protein blocking experiments were carried out in which anti-human TGFBIp was pre-incubated with an equimolar amount (1 μM) of human recombinant TGFBIp (rTGFBIp, R&D Systems, Minneapolis, MN) for 1 hr at room temperature prior to use in western blots.

Cell attachment assay

96-well plates were pre-coated with 10 μg/ml rat tail collagen type I (100 μl/well) (Sigma-Aldrich, St. Louis, MO) and incubated overnight at 4 °C. After removing excess liquid from the wells, the plate was UV sterilized under a culture hood overnight and the wells rinsed with PBS. HSFs were resuspended in DMEM/1× a/a containing 0.5% FBS at a concentration of 2000 cells/200 μl containing 0 - 50 μg/ml of bovine serum albumin (BSA, Sigma, St. Louis, MO), fibronectin (FN, Sigma, St. Louis, MO) or rTGFBIp. For antibody blocking experiments, an equimolar amount of anti-TGFBIp antibody (50 μg/ml, R&D Systems, Minneapolis, MN) was pre-incubated with rTGFBIp (25 μg/ml, R&D Systems, Minneapolis, MN) for 1 hr at room temperature prior to the addition of cells. Cells were immediately seeded in triplicate (2000 cells/well) to collagen-coated plates and permitted to attach for 45 min at 37 °C (95% air containing 5% CO_2) before gently rinsing off the unattached cells twice with PBS. Finally,

toluidine blue [150 μl; 0.5% toluidine blue stain in 4% paraformaldehyde (wt/vol)] was added to each well for 5 min at room temperature, removed, and then wells were rinsed three times with milliQ water before solubilizing with 1% SDS (250 μl). Cell numbers were determined by reading absorbance at 595 nm using a platereader (Biorad, Hercules, CA) and comparing to a standard curve prepared from 0 – 10,000 cells/well.

TGFBIp binding assay using biotinylated rTGFBIp

rTGFBIp (R&D Systems, Minneapolis, MN) was biotinylated using the EZ-Link® Micro Sulfo-NHS-Biotinylation Kit (Pierce, Rockford, IL) according to the manufacturer's instructions. Briefly, 11 mM Sulfo-NHS-biotin in PBS was added in a 50-fold molar excess to rTGFBIp (6 μl, 11 mM Sulfo-NHS-biotin in PBS/per 500 μl rTGFBIp) and incubated while rotating at room temperature for 1 hr. During the incubation, a Zeba desalt spin column was prepared by centrifugation at 1000 × g for 2 min (Sorvall® RT 6000D, DuPont, Hoffman Estates, IL) to remove the storage buffer and equilibrate the column (3 washes with 1 ml PBS). Following the 1 hr incubation, the protein-biotin mixture was placed onto the column and allowed to absorb into the resin before centrifugation at 1000 × g for 2 min. The flow through, consisting of purified biotinylated rTGFBIp, was collected and stored at -20 °C until use. The bicinchoninic acid (BCA) protein assay (Pierce Chemical, Rockford, IL) was used to determine the concentration of biotinylated rTGFBIp using the NanoDrop® ND-1000 spectrophotometer (NanoDrop Technologies, Wilmington, DE) as previously described.[44]

Binding assays were performed as described previously with slight modifications.[51-53] HSFs were suspended in serum-free medium (DMEM + 1× a/a) at a density of 1×10^5 cells/ml, centrifuged at 1000 rpm for 5 min at 4 °C, washed in ice-cold PBS, recentrifuged at 1000 rpm for 5 min, and reconstituted in serum-free medium containing biotinylated rTGFBIp (0 – 50 μg/ml) and incubated at 4 °C for 5 hrs with rotation. Next, the cells were washed three times with ice-cold PBS, and lysed by the addition of 100 μl cell lysis buffer. Equal amounts (10 μl) of protein from each sample were separated on a 10% SDS-PAGE gel and then transferred to a nitrocellulose membrane. Biotinylated rTGFBIp was visualized by incubation of membranes with streptavidin conjugated to alkaline phosphatase (1:3000, Sigma, St. Louis, MO). Biotinylated and nonbiotinylated rTGFBIp were also visualized by incubating the blots with anti-TGFBIp antibody (1:500) overnight at 4 °C followed by incubation with anti-goat IgG conjugated to alkaline phosphatase and imaged with CDP-*Star* chemiluminescent substrate. Following detection of biotinylated rTGFBIp, blots were stripped with Restore™ Plus Western Blot Stripping Buffer (Pierce, Rockford, IL) according to the manufacturer's protocol, and reprobed with α-tubulin antibody (1:10000) for an internal control. For some experiments, 1 ml of the HSF cell suspension was preincubated with anti-mouse αvβ3 or anti-mouse αvβ5 integrin antibody (final concentration 0 – 10 μg/ml; Millipore, Temecula, CA) for 1 hr at 4 °C with rotation prior to washing three times with ice-cold PBS and incubation with biotinylated rTGFBIp.

Additionally, competitive binding experiments were carried out in which HSFs were incubated with nonbiotinylated rTGFBIp (0 – 50 μg/ml) in serum-free medium for 3 hrs at 4 °C, washed in ice-cold PBS, and then incubated with 10 μg/ml biotinylated rTGFBIp for 3 hrs at 4 °C. Cells were washed again, lysed, and biotinylated and total rTGFBIp were detected by western blot using streptavidin and anti-TGFBIp, respectively, as described above.

Flow cytometric analysis

To confirm the expression of a specific integrin(s) on the surface of HSFs, fluorescence-activated cell sorter analyses were performed. HSFs were grown to confluency in serum-containing medium and detached from plates by treatment with HBSS containing 0.05% EDTA, as described previously. The cells were rinsed twice in wash buffer (PBS containing

0.1% BSA), resuspended in wash buffer at a concentration of 1×10^5 cells/ml, and incubated for 1 hr at 4 °C with 4 μg/ml of monoclonal mouse anti-integrin αvβ3 (clone# LM609) or anti-αvβ5 (clone# P1F6) antibodies (Millipore, Temecula, CA). Cells were pelleted by centrifugation at 1000 rpm for 5 min, supernatants removed and cell pellets rinsed three times with wash buffer. Cells were then incubated in the dark for 1 hr at 4 °C with 10 μg/ml Alexa Fluor® 568 rabbit anti-mouse IgG (Molecular Probes, Eugene, OR). Cells were pelleted, washed again and analyzed on a FACSCalibur flow cytometry system (Becton Dickinson, San Jose, CA) at the University of Oklahoma Health Sciences Center, Flow and Image Cytometry Core Laboratory (Director, Jim Henthorn, Oklahoma City, OK).

Immunofluorescence

HSFs were grown in 100 mm dishes in serum-containing medium, detached and seeded onto 12 mm round coverslips in a 24-well culture dish in serum-containing medium (Corning Incorporated, Corning, NY). Following 24 hrs of incubation at 37 °C, the culture media was aspirated and the coverslips washed twice with PBS containing 0.5 mM $CaCl_2$ and $MgCl_2$ (PBS++) to remove unattached cells. Cells were then fixed in 4% paraformaldehyde in wash buffer for 5 min at room temperature, followed by a 15 min incubation in 4% paraformaldehyde on ice before washing 3× for 5 min with wash buffer. Coverslips containing fixed cells were incubated with non-immune mouse IgG, anti-TGFBIp, anti-αvβ3 or anti-αvβ5 antibodies (1:100 dilution in PBS++ containing 0.1% FBS) for 1 hr at room temperature. After washing, the coverslips were incubated with the appropriate secondary antibody conjugated to AlexaFluor 488 or AlexaFluor 568 (1:200 dilution in PBS++ containing 0.1% FBS) in the dark for 1 hr at room temperature. After washing 6× for 10 min with PBS++ the coverslips were rinsed in milliQ water then mounted to slides using ProLong® Gold antifade reagent containing DAPI (Invitrogen, Eugene, OR). Cells were viewed using a Fluoview FV1000 confocal laser scanning microscope (Olympus America Inc., Melville, NY).

Statistical analysis

Statistical comparisons were made using the Student's *t*-test for unmatched pairs with the assistance of GraphPad Prism version 4.03 for Windows (GraphPad Software, San Diego, CA). Nonlinear regression analysis using the sigmoidal dose response equation for variable slopes was used to determine the required concentration to reach 50% inhibition (IC_{50}) using GraphPad Prism.

Results

TGFBI/TGFBIp expression by HSFs

TGFBI gene expression by HSFs was confirmed by RT-PCR using human primers specific to *TGFBI* together with the housekeeping gene, cyclophilin A (*PPIA*), which served as the positive control. Following electrophoresis on a 1.5% agarose gel, single bands at 373 bp and 300 bp could be detected for *TGFBI* and cyclophilin, respectively (Figure 1A). No bands were observed when reverse transcriptase was omitted from the PCR reactions (data not shown), indicating that PCR amplicons were not the result of DNA contamination. TGFBIp expression was evaluated in scleral fibroblast cell lysates and in culture supernatants by western blot. A 68 kDa band was observed in the conditioned media (Figure 1B, 1× media, top panel). A faint 68 kDa band (Figure 1B, 10× cell lysates, top panel), could be identified on 10× concentrated cell lysates, and no bands were detected in culture media in the absence of HSFs (Figure 1B, top panel; DMEM + 0.05% FBS). All bands were abolished when rTGFBIp was preincubated with an equimolar amount (1 μM) of the primary anti-TGFBIp antibody, thereby confirming the specificity of the antibody used (Figure 1B, middle panel). Comparison of TGFBIp in scleral fibroblast culture supernatants (1× conditioned media) with a standard curve prepared

from rTGFBIp (0.5 – 5.0 μg) indicated that HSFs secreted abundant levels of TGFBIp [~4 μg/ml/48 hrs (~833 ng/hr), Figure 1C)].

TGFBIp modulates HSF adhesion to collagen

To assess the effects of TGFBIp on cell adhesion to collagen-type I, primary HSFs were plated on collagen-coated 96-well plates in the presence of bovine serum albumin (BSA), fibronectin (FN), rTGFBIp and/or anti-TGFBIp antibody (Figure 2). rTGFBIp significantly inhibited HSF attachment at concentrations of 25 μg/ml (-32% ± 12.6, $p < 0.05$) and 50 μg/ml (-47% ± 2.1, $p < 0.01$) in a dose-dependent manner as compared to BSA alone (Figure 2A). HSFs treated with antibody-neutralized rTGFBIp (25 μg/ml rTGFBIp + 50 μg/ml anti-TGFBIp) showed a significant increase in attachment to collagen as compared to cells treated with rTGFBIp alone (+34% ± 5.0, $p < 0.01$), and no significant difference as compared to BSA (+9% ± 7.4, $p = 0.29$). HSF attachment to collagen in the presence of anti-TGFBIp alone (50 μg/ml) was similar to cell attachment to BSA-treated collagen-coated wells (+7% ± 2.1, $p = 0.20$).

The effect of TGFBIp on cell adhesion was also assessed using human foreskin fibroblasts (HFFs) and human corneal stromal fibroblasts (HCFs). The addition of rTGFBIp did not significantly inhibit or promote the attachment of HFFs to collagen type I as compared to BSA (-4% ± 13.5, $p = 0.50$; Figure 2C); however, treatment with rTGFBIp together with equimolar amounts of anti-TGFBIp showed a significant decrease in attachment as compared to BSA (-28% ± 3.8, $p < 0.01$). Similarly, rTGFBIp did not appear to affect HCF attachment to collagen type I as compared to BSA (+37% ± 23.7, $p = 0.24$; Figure 2D); in contrast to HFFs, treatment of HCFs with antibody neutralized rTGFBIp did not appear to affect attachment as compared to BSA (-22% ± 22.7, $p = 0.51$). These results demonstrate that TGFBIp inhibits HSF adhesion to collagen type I, but does not affect the adhesion of HFF or HCF to collagen. Previous studies have demonstrated that when corneal keratocytes are grown in the presence of serum, they take on a fibroblast phenotype, actively proliferate, and do not express the keratocyte-specific protein, keratocan.[50,54-56] Based on our growth conditions and the phenotype of the cells (Figure 2D–inset), the corneal cells used in these cell attachment studies most closely resemble corneal fibroblasts, as opposed to corneal keratocytes or myofibroblasts.

TGFBIp binds to the surface of HSFs

Biotinylation of rTGFBIp (100 ng) did not alter the expected 68 kD band as compared to rTGFBIp (100 ng) when probed with streptavidin conjugated to alkaline phosphatase (Figure 3A). To determine whether TGFBIp directly binds to the surface of HSFs, HSFs were incubated with biotinylated rTGFBIp (0 – 50 μg/ml), and specific binding was determined by visualizing biotinylated rTGFBIp with streptavidin-alkaline phosphatase using western blot analysis (Figure 3B). Biotinylated rTGFBIp was observed as a single band migrating at 68 kD (arrowhead). In addition, a biotinylated higher molecular weight band of 136-140 kD was detected on blots, most likely due to nonspecific binding of streptavidin to a protein(s) in the cell lysates. Binding of biotinylated rTGFBIp to HSFs was saturable at concentrations ≥ 0.37 nM (25 μg/ml; Bmax) and 50% maximal binding was achieved at 0.15 nM (10 μg/ml).

To investigate specificity of TGFBIp binding to the HSF cell surface, competitive binding assays were performed by assessing biotinylated 0.15 nM rTGFBIp (10 μg/ml) binding to HSFs in the presence of increasing amounts of nonbiotinylated competitor rTGFBIp [0 – 0.74 nM (50 μg/ml)] (Figure 4A). The concentration of biotinylated rTGFBIp used in competitive binding assays was determined based on the estimated Km for rTGFBIp binding (0.185 nM). Analysis of band intensities following the competitive binding assays indicated that the concentration of rTGFBIp required for 50% inhibition (IC_{50}) of binding to HSFs in vitro was . 03 nM (Figure 4B). Ideally, half of the data points on the IC_{50} curve are above the IC_{50} value and half are below the IC_{50} value, but unfortunately this did not occur in our experiments.

Therefore additional points (inhibitor concentrations) should be included for a more accurate IC_{50} determination. However, based on the criteria that the maximum inhibition is >50%, we elected to include these results as shown.

TGFBIp binds to specific integrins expressed on the surface of HSFs

Flow cytometry was performed using monoclonal antibodies specific for αvβ3and αvβ5 integrins. Compared to the nonimmune IgG isotype control (Figure 5A), specific labeling for both αvβ3 (Figure 5B) and αvβ5 (Figure 5C) integrins were detected on the surface of HSFs ($p < 0.05$) with the anti-αvβ5 antibody generating a stronger signal than anti-αvβ3 (Figure 5D). Binding of biotinylated rTGFBIp to HSFs in the presence of anti-αvβ3 (Figure 6A) and anti-αvβ5 (Figure 6B) antibody was significantly inhibited at concentrations of 1-10 μg/ml (60–84% and 42–56%, respectively). The anti-αvβ5 antibody was less effective at inhibiting the binding of biotinylated rTGFBIp, but still demonstrated a significant decrease in binding at concentrations ≥1 μg/ml ($p < 0.05$). Following the binding assays, both anti-αvβ3 and anti-αvβ5 integrin antibodies were confirmed to bind on the surface of HSFs by detection of mouse IgG with anti-mouse IgG conjugated to alkaline phosphatase using western blot analysis (data not shown).

Expression of TGFBIp and integrins in cultured HSFs

The distribution of TGFBIp, αvβ3 and αvβ5 was assessed on the surface of cultured HSFs using immunocytochemistry (Figure 7). TGFBIp was predominantly expressed on the cell surface, between adjacent cells, with minimal intracellular expression. Integrins αvβ3 and αvβ5 appeared to colocalize with TGFBIp on the cell surface (merged images). The acellular staining present in regions of Figure 7 most likely represent areas where cells had been artifactually detached during the procedure. Negative control sections were processed in parallel by incubation with secondary antibody only, or non-immune mouse IgG, and showed no significant fluorescence signal.

Discussion

TGFBIp is primarily expressed in collagen-rich tissues in association with various extracellular matrix components as well as the cell surface, suggesting an organizational and structural role. TGFBIp is ~77 kD in size and contains a NH_2-terminal signal peptide sequence (residues 1-23) that is proteolytically processed during export to the extracellular matrix, rendering the protein a 68 kD isoform.[46] Additionally, this protein contains 11 cysteine residues mainly clustered in the NH_2-terminal region (EMI domain), four highly conserved fasciclin-like (FAS) domains, and a COOH-terminal Arg-Gly-Asp (RGD) sequence.[45-46,57-58] Due to the structural components of the protein, the presence of the FAS and RGD domains indicate that TGFBIp may play a functional role in cell adhesion.[59-62] In both the marmoset and human sclera, TGFBIp expression has only recently been described.[44] To elucidate the role of TGFBIp within the scleral extracellular matrix, studies in our laboratory have focused on the cell-matrix interactions using an in vitro system.

Results in the present study demonstrate that HSFs express *TGFBI*, and that its protein product, TGFBIp, is secreted into the culture medium in abundant quantities by HSFs, in vitro (~833 ng/hr). Relatively little TGFBIp remained attached to the cell surface or was contained intracellularly, as demonstrated by western blot analyses of the 10× cell lystate (Figure 1B). Secreted TGFBIp was detected as a single 68 kD band (Figure 1B), but a higher molecular weight band (~120 kD) was present in cell lysates containing biotinylated rTGFBIp when probed with streptavidin-AP (Figures 3, 4 and 6). Since this band was not present when blots were probed with anti-TGFBIp, we suspect this band represents nonspecific binding of streptavidin to a protein in the cell lysates.[63-64]

We previously demonstrated the inhibitory effect of TGFBIp on the attachment of HSFs in a solid-phase cell adhesion assay.[44] The present study demonstrates that TGFBIp mediates decreased HSF attachment to collagen-type I in a fluid-phase assay. Previous studies have shown TGFBIp supports cell adhesion in many cell types including corneal fibroblasts,[65-67] foreskin fibroblasts,[62] bladder fibroblasts,[68] U87 astrocytoma cells,[69] skeletal muscle cells,[70] proximal tubular epithelial cells,[71] osteoblasts,[53] keratinocytes,[72] SMMC-7721 hepatoma cells[73] and peritoneal mesothelial cells.[74] Conversely, it has been reported to inhibit cell adhesion in human neuroblastoma cells,[75] A549 lung adenocarcinoma cells, HeLa cells, and WI-38 cells.[46] In the present study, we determined that rTGFBIp inhibited the attachment of HSFs to collagen (-32%, $p < 0.01$), and this effect was restored after neutralizing rTGFBIp with equimolar amounts of anti-TGFBIp as compared to BSA (+9%, $p = 0.29$, Figure 2B). Additionally, the short incubation period (45 min) allotted for cell attachment suggests that the anti-adhesive effect of rTGFBIp on HSFs is not a result of decreased cell proliferation. In agreement to previous reports, we observed that rTGFBIp does not inhibit attachment to collagen type I using both HFFs (-4%, $p = 0.50$) (Figure 2C) and HCFs (+37%, $p = 0.24$) (Figure 2D), as compared to BSA. However, a significant decrease in attachment to collagen type I was observed in HFFs treated with antibody-neutralized rTGFBIp as compared to cells treated with BSA alone (-28%, $p < 0.01$). Since the attachment of HFFs to collagen type I was not affected by treatment with anti-TGFBIp alone, we speculate that the TGFBIp antibody:antigen complexes generated in vitro must be anti-adhesive to HFFs in our attachment assays. Nevertheless, the finding that TGFBIp inhibits attachment of HSFs to collagen type I, but not HFFs or HCFs suggests multiple functional roles of TGFBIp among different cell and tissue types, and that the anti-adhesive effect of TGFBIp may be fairly specific for HSFs. In contrast to TFGBIp, FN enhanced attachment of HSFs to collagen type I. We speculate that FN may be attaching to HSFs via the αvβ5 integrin receptor, as FN has been demonstrated to bind to a variety of cell types by this receptor,[76-78] and we have demonstrated this integrin on the HSF cell surface. Since rTGFBIp was shown to bind to HSFs by both αvβ3 and αvβ5, it is likely that rTGFBIp may block adhesion of HSFs to FN as well; however these experiments were not carried out in the present study.

Several studies have reported that TGFBIp can bind to the surface of cells in connective tissue rich matrices to modulate their adhesive properties via cell-specific integrins.[47,53,62,68-69,73,79-80] In the present study, binding assays using biotinylated rTGFBIp (0 - 50 μg/ml) confirmed that TGFBIp binds directly to the surface of HSFs, and binding was saturable at concentrations ≥ 0.37 nM with an IC_{50} of .03 nM. Interestingly, this relatively high affinity binding of TGFBIp to the HSF cell surface described here is similar to that described for the affinity of TGF-β1 latency-associated peptide binding to αvβ6 integrin receptors (18 pM).[81] Integrins implicated in binding TGFBIp to the cell surface include, α1β1,[82] α3β1,[72-73,83-84] αVβ3,[53,74] αVβ5,[85,53] α7β1[70] and α6β4.[69] The Arg-Gly-Asp (RGD) sequence present on the C-terminal region of TGFBIp is thought to act as a universal ligand recognition site for integrins; however, the attachment and spreading of cells to TGFBIp does not solely require the RGD sequence, but can occur via the fasciclin-like domains.[82] In the present study, flow cytometry and immunocytochemistry using monoclonal antibodies to the integrins αvβ3 and αvβ5 were utilized to identify the expression of αvβ3 and αvβ5 on the HSF cell surface. Based on the mean fluorescence intensities, the relative expression level of αvβ5 appeared more elevated than that of αvβ3. Therefore, αvβ5 may function predominantly in mediating the binding of TGFBIp to HSFs. In addition to our findings, two previous reports in tree shrew, both in vitro and in vivo, have demonstrated mRNA expression of the integrin subunits, α1, α3 and β1 in scleral fibroblasts.[86-87] Taken together, these results suggest that scleral fibroblasts express a variety of integrin subunits, a subset of which are translated and expressed as integrin receptors on the cell surface.

To identify whether αvβ3 and/or αvβ5 integrins play a role in TGFBIp binding to the surface of HSFs, additional binding assays were conducted following pre-incubation with specific antibodies to the αvβ3 and αvβ5 integrins (0 – 10 μg/ml). Binding of biotinylated rTGFBIp was significantly inhibited in a dose-dependent manner by the addition of either anti-αvβ3 or anti-αvβ5. This disruption of interactions between TGFBIp and HSFs by function-blocking antibodies specific for αvβ3 and αvβ5 integrins suggests that both αvβ3 and αvβ5 mediate some of the binding of TGFBIp to the HSF cell surface, and therefore have the potential to regulate attachment.

The mechanism by which TGFBIp modulates cell attachment is not well understood. The results of this study suggest that both αvβ3 and αvβ5 integrins are functional receptors for TGFBIp on the scleral cell membrane. The expression and activity of integrin downstream signaling molecules FAK and paxillin show a positive correlation with TGFBIp expression in human hepatoma cells, suggesting that TGFBIp may alter cell attachment via an integrin-mediated signaling cascade that may lead to cytoskeleton reorganization.[73] Alternatively, the binding of TGFBIp to the HSF cell surface may sterically inhibit cell attachment to collagen type I as has been demonstrated for hexabrachion (tenascin)[88] and thrombospondin.[89-91] In support of integrin-mediated signaling, FN was shown in the present study to enhance attachment of HSFs to collagen type I. Since FN is well known to mediate its pro-adhesive property via the αvβ3 integrin receptor(s), it is possible that interaction differences between TGFBIp, FN, and the αvβ3 integrin receptor result in distinct downstream signaling pathways that lead to increased adhesion in one condition (FN), and decreased adhesion in another (TGFBIp). Moreover, differences in integrin subunit expression between different cell types may initiate divergent signaling cascades that result in TGFBIp being pro-adhesive for some cell types and anti-adhesive for others.

The highly regulated viscoelastic nature of the sclera has been speculated to occur as a result of slippage (creep) of the lamellae across each other at the cell-lamellae interface,[33] and is highly correlated with the rate of ocular elongation during myopia development as well as during decelerated ocular growth during recovery or compensation for plus lenses.[33-34] Therefore, we speculate that changes in scleral ECM remodeling and cell-matrix interactions at the lamellae interface may modulate viscoelasticity in a variety of ocular growth states. The results presented in this paper suggest that TGFBIp is one molecule that may regulate the attachment of HSFs to collagen type I at the fibroblast-lamellae interface thereby regulating the amount of lamellar slippage, scleral viscoelasticity, and the rate of scleral elongation. Interestingly, significant increases in *TGFBI* mRNA transcription levels were recently observed to occur in the scleras of tree shrew eyes undergoing minus-lens compensation.[92] These results, together with the results of the present study suggest that changes in scleral levels of TGFBIp may act to regulate ocular elongation via modulation of cell-matrix interactions.

The molecular mechanisms which regulate the scleral ECM remodeling, scleral distensibility and axial length are poorly understood. The results of the present study suggest that TGFBIp may limit cell-matrix interactions between HSFs and collagen type I via integrin receptors. Additional functional in vivo studies are required to elucidate the role of TGFBIp, αvβ3, and αvβ5 in the sclera and how these proteins may be involved in scleral ECM remodeling during normal ocular growth and myopia development.

Acknowledgments

The authors wish to acknowledge Brian dela Cruz and Rachel Folger for their technical assistance. The authors also wish to thank David M. Sherry and Brian P. Ceresa (OUHSC, Department of Cell Biology) for their helpful discussions and suggestions pertaining to this manuscript. This work was supported by National Eye Institute Grants R01 EY09391 (J.A.S.) and the Macula Vision Research Foundation (J.A.S.).

Support: National Eye Institute Grants R01 EY09391 (JAS) and the Macula Vision Research Foundation (JAS)

References

1. Marshall GE, Konstas AG, Lee WR. Collagens in the aged human macular sclera. Curr Eye Res 1993;12:143–53. [PubMed: 8449025]
2. White J, Werkmeister JA, Ramshaw JA, Birk DE. Organization of fibrillar collagen in the human and bovine cornea: collagen types V and III. Connect Tissue Res 1997;36:165–74. [PubMed: 9512886]
3. Gentle A, Liu Y, Martin JE, Conti GL, McBrien NA. Collagen gene expression and the altered accumulation of scleral collagen during the development of high myopia. J Biol Chem 2003;278:16587–94. [PubMed: 12606541]
4. Tamura Y, Konomi H, Sawada H, Takashima S, Nakajima A. Tissue distribution of type VIII collagen in human adult and fetal eyes. Invest Ophthalmol Vis Sci 1991;32:2636–44. [PubMed: 1869415]
5. Wessel H, Anderson S, Fite D, Halvas E, Hempel J, SundarRaj N. Type XII collagen contributes to diversities in human corneal and limbal extracellular matrices. Invest Ophthalmol Vis Sci 1997;38:2408–22. [PubMed: 9344363]
6. Sandberg-Lall M, Hägg PO, Wahlström I, Pihlajaniemi T. Type XIII collagen is widely expressed in the adult and developing human eye and accentuated in the ciliary muscle, the optic nerve and the neural retina. Exp Eye Res 2000;70:401–10. [PubMed: 10865988]
7. Rada, JA.; Johnson, JM. Sclera. Cornea. Krachmer, J.; Mannis, M.; Holland, E., editors. Mosby; St Louis: 2004.
8. Rada JA, Achen VR, Perry CA, Fox PW. Proteoglycans in the human sclera. Evidence for the presence of aggrecan. Invest Ophthalmol Vis Sci 1997;38:1740–51. [PubMed: 9286262]
9. Corpuz LM, Funderburgh JL, Funderburgh ML, Bottomley GS, Prakash S, Conrad GW. Molecular cloning and tissue distribution of keratocan. Bovine corneal keratan sulfate proteoglycan 37A. J Biol Chem 1996;271:9759–63. [PubMed: 8621655]
10. Ying S, Shiraishi A, Kao CW, et al. Characterization and expression of the mouse lumican gene. J Biol Chem 1997;272:30306–13. [PubMed: 9374517]
11. Rada JA, Achen VR, Penugonda S, Schmidt RW, Mount BA. Proteoglycan composition in the human sclera during growth and aging. Invest Ophthalmol Vis Sci 2000a;41:1639–48. [PubMed: 10845580]
12. Johnson JM, Young TL, Rada JA. Small leucine rich repeat proteoglycans (SLRPs) in the human sclera: identification of abundant levels of PRELP. Mol Vis 2006;12:1057–66. [PubMed: 17093390]
13. Marshall GE. Human scleral elastic system: an immunoelectron microscopic study. Br J Ophthalmol 1995;79:57–64. [PubMed: 7533533]
14. Frost MR, Norton TT. Differential protein expression in tree shrew sclera during development of lens-induced myopia and recovery. Mol Vis 2007;13:1580–8. [PubMed: 17893659]
15. Rada JA, Shelton S, Norton TT. The sclera and myopia. Exp Eye Res 2006;82:185–200. [PubMed: 16202407]
16. Curtin BJ, Teng CC. Scleral changes in pathological myopia. Trans Am Acad Ophthalmol Otolaryngl 1957;62:777–790.
17. Curtin BJ, Iwamoto T, Renaldo DP. Normal and staphylomatous sclera of high myopia: An electron microscopic study. Arch Ophthalmol 1979;97:912–915. [PubMed: 444126]
18. Avetisov ES, Savitskaya NF, Vinetskaya MI, Iomdina EN. A study of biochemical and biomechanical qualities of normal and myopic eye sclera in humans of different age groups. Metab Pediatr Syst Ophthalmol 1983;7:183–8. [PubMed: 6678372]
19. Troilo D, Wallman J. The regulation of eye growth and refractive state: an experimental study of emmetropization. Vision Res 1991;31:1237–50. [PubMed: 1891815]
20. Norton TT, Rada JA. Reduced extracellular matrix in mammalian sclera with induced myopia. Vision Res 1995;35:1271–81. [PubMed: 7610587]
21. Siegwart JT Jr, Norton TT. Steady state mRNA levels in tree shrew sclera with form-deprivation myopia and during recovery. Invest Ophthalmol Vis Sci 2001;42:1153–9. [PubMed: 11328721]
22. Siegwart JT Jr, Norton TT. The time course of changes in mRNA levels in tree shrew sclera during induced myopia and recovery. Invest Ophthalmol Vis Sci 2002;43:2067–75. [PubMed: 12091398]

23. Siegwart JT Jr, Norton TT. Selective regulation of MMP and TIMP mRNA levels in tree shrew sclera during minus lens compensation and recovery. Invest Ophthalmol Vis Sci 2005;46:3484–92. [PubMed: 16186323]
24. Troilo D, Nickla DL, Mertz JR, Summers Rada JA. Change in the synthesis rates of ocular retinoic acid and scleral glycosaminoglycan during experimentally altered eye growth in marmosets. Invest Ophthalmol Vis Sci 2006;47:1768–77. [PubMed: 16638980]
25. Norton TT. Experimental myopia in tree shrews. Ciba Found Symp 1990;155:178–94. [PubMed: 2088676]
26. McBrien NA, Gentle A. The role of visual information in the control of scleral matrix biology in myopia. Curr Eye Res 2001;23:313–9. [PubMed: 11910519]
27. McBrien NA, Lawlor P, Gentle A. Scleral remodeling during the development of and recovery from axial myopia in the tree shrew. Invest Ophthalmol Vis Sci 2000;41:3713–9. [PubMed: 11053267]
28. Rada JA, Nickla DL, Troilo D. Decreased proteoglycan synthesis associated with form deprivation myopia in mature primate eyes. Invest Ophthalmol Vis Sci 2000b;41:2050–8. [PubMed: 10892842]
29. Jobling AI, Nguyen M, Gentle A, McBrien NA. Isoform-specific changes in scleral transforming growth factor-beta expression and the regulation of collagen synthesis during myopia progression. J Biol Chem 2004;279:18121–6. [PubMed: 14752095]
30. Rada JA, Brenza HL. Increased latent gelatinase activity in the sclera of visually deprived chicks. Invest Ophthalmol Vis Sci 1995;36:1555–65. [PubMed: 7601636]
31. Jones BE, Thompson EW, Hodos W, Waldbillig RJ, Chader GJ. Scleral matrix metalloproteinases, serine proteinase activity and hydrational capacity are increased in myopia induced by retinal image degradation. Exp Eye Res 1996;63:369–81. [PubMed: 8944544]
32. Guggenheim JA, McBrien NA. Form-deprivation myopia induces activation of scleral matrix metalloproteinase-2 in tree shrew. Invest Ophthalmol Vis Sci 1996;37:1380–95. [PubMed: 8641841]
33. Siegwart JT Jr, Norton TT. Regulation of the mechanical properties of tree shrew sclera by the visual environment. Vision Res 1999;39:387–407. [PubMed: 10326144]
34. Phillips JR, Khalaj M, McBrien NA. Induced myopia associated with increased scleral creep in chick and tree shrew eyes. Invest Ophthalmol Vis Sci 2000;41:2028–34. [PubMed: 10892839]
35. McBrien NA, Gentle A. Role of the sclera in the development and pathological complications of myopia. Prog Retin Eye Res 2003;22:307–38. [PubMed: 12852489]
36. Wallman J, Gottlieb MD, Rajaram V, Fugate-Wentzek LA. Local retinal regions control local eye growth and myopia. Science 1987;237:73–7. [PubMed: 3603011]
37. Miles FA, Wallman J. Local ocular compensation for imposed local refractive error. Vision Res 1990;30:339–49. [PubMed: 2336793]
38. Wildsoet C, Wallman J. Choroidal and scleral mechanisms of compensation for spectacle lenses in chicks. Vision Res 1995;35:1175–94. [PubMed: 7610579]
39. Troilo D, Gottlieb MD, Wallman J. Visual deprivation causes myopia in chicks with optic nerve section. Curr Eye Res 1987;6:993–9. [PubMed: 3665562]
40. Wallman J, Winawer J. Homeostasis of eye growth and the question of myopia. Neuron 2004;43:447–68. [PubMed: 15312645]
41. Wallman J, Wildsoet C, Xu A, et al. Moving the retina: choroidal modulation of refractive state. Vision Res 1995;35:37–50. [PubMed: 7839608]
42. Marzani D, Wallman J. Growth of the two layers of the chick sclera is modulated reciprocally by visual conditions. Invest Ophthalmol Vis Sci 1997;38:1726–39. [PubMed: 9286261]
43. Rada JA, Palmer L. Choroidal regulation of scleral glycosaminoglycan synthesis during recovery from induced myopia. Invest Ophthalmol Vis Sci 2007;48:2957–66. [PubMed: 17591860]
44. Shelton L, Troilo D, Lerner MR, Gusev Y, Brackett DJ, Rada JS. Microarray analysis of choroid/RPE gene expression in marmoset eyes undergoing changes in ocular growth and refraction. Mol Vis 2008;14:1465–1479. [PubMed: 18698376]
45. Skonier J, Neubauer M, Madisen L, Bennett K, Plowman GD, Purchio AF. cDNA cloning and sequence analysis of beta ig-h3, a novel gene induced in a human adenocarcinoma cell line after treatment with transforming growth factor-beta. DNA Cell Biol 1992;11:511–22. [PubMed: 1388724]

46. Skonier J, Bennett K, Rothwell V, et al. βig-h3: A transforming growth factor-β-responsive gene encoding a secreted protein that inhibits cell attachment in vitro and suppresses the growth of CHO cells in nude mice. DNA and Cell Biology 1994;13:571–584. [PubMed: 8024701]
47. Thapa N, Lee BH, Kim IS. TGFBIp/βig-h3 protein: A versatile matrix molecule induced by TGF-β. Int J Biochem Cell Bio 2007;39:2183–2194. [PubMed: 17659994]
48. Shelton L, Rada JS. Effects of cyclic mechanical stretch on extracellular matrix synthesis by human scleral fibroblasts. Exp Eye Res 2007;84:314–22. [PubMed: 17123515]
49. Rada JA, Thoft RA, Hassell JR. Increased aggrecan (cartilage proteoglycan) production in the sclera of myopic chicks. Dev Biol 1991;147:303–12. [PubMed: 1916012]
50. Hassell JR, Schrecengost PK, Rada JA, SundarRaj N, Sossi G, Thoft RA. Biosynthesis of stromal matrix proteoglycans and basement membrane components by human corneal fibroblasts. Invest Ophthalmol Vis Sci 1992;33:547–57. [PubMed: 1544783]
51. Maile LA, Imai Y, Clarke JB, et al. Insulin-like growth factor I increases αVβ3 affinity by increasing the amount of integrin-associated protein that is associated with non-raft domains of the cellular membrane. J Biol Chem 2002;277:1800–1805. [PubMed: 11707450]
52. Nam JO, Kim JE, Jeong HW, et al. Identification of the αvβ3 integrin-interacting motif of βig-h3 and its anti-angiogenic effect. J Biol Chem 2003;278:25902–25909. [PubMed: 12704192]
53. Thapa N, Kang KB, Kim IS. Beta ig-h3 mediates osteoblast adhesion and inhibits differentiation. Bone 2005;36:232–242. [PubMed: 15780949]
54. Jester JV, Huang J, Barry-Lane PA, Kao WW, Petroll WM, Cavanagh HD. Transforming growth factor(beta)-mediated corneal myofibroblast differentiation requires actin and fibronectin assembly. Invest Ophthalmol Vis Sci 1999;40:1959–1967. [PubMed: 10440249]
55. Beales MP, Funderburgh JL, Jester JV, Hassell JR. Proteoglycan synthesis by bovine keratocytes and corneal fibroblasts: maintenance of the keratocyte phenotype in culture. Invest Ophthalmol Vis Sci 1999;40:1658–1663. [PubMed: 10393032]
56. Ryan DG, Taliana L, Sun L, Wei ZG, Masur SK, Lavker RM. Involvement of S100A4 in stromal fibroblasts of the regenerating cornea. Invest Ophthalmol Vis Sci 2003;44:4255–62. [PubMed: 14507869]
57. Hashimoto K, Noshiro M, Ohno S, et al. Characterization of a cartilage-derived 66-kDa protein (RGD-CAP/beta ig-h3) that binds to collagen. Biochim Biophys Acta 1997;1355:303–14. [PubMed: 9061001]
58. Kawamoto T, Noshiro M, Shen M, et al. Structural and phylogenetic analyses of RGD-CAP/beta ig-h3, a fasciclin-like adhesion protein expressed in chick chondrocytes. Biochim Biophys Acta 1998;1395:288–292. [PubMed: 9512662]
59. Saiki I, Iida J, Murata J, et al. Inhibition of the metastasis of murine malignant melanoma by synthetic polymeric peptides containing core sequences of cell-adhesive molecules. Cancer Res 1989;49:3815–22. [PubMed: 2736523]
60. Elkins T, Hortsch M, Bieber AJ, Snow PM, Goodman CS. Drosophila fasciclin I is a novel homophilic adhesion molecule that along with fasciclin III can mediate cell sorting. J Cell Biol 1990;110:1825–32. [PubMed: 2335571]
61. Elkins T, Zinn K, McAllister L, Hoffmann FM, Goodman CS. Genetic analysis of a Drosophila neural cell adhesion molecule: interaction of fasciclin I and Abelson tyrosine kinase mutations. Cell 1990;60:565–75. [PubMed: 2406026]
62. LeBaron RG, Bezverkov KI, Zimber MP, Pavelec R, Skonier J, Purchio AF. Beta IG-H3, a novel secretory protein inducible by transforming growth factor-beta, is present in normal skin and promotes the adhesion and spreading of dermal fibroblasts in vitro. J Invest Dermatol 1995;104:844–9. [PubMed: 7738366]
63. Alon R, Bayer EA, Wilcheck M. Cell-adhesive properties of streptavidin are mediated by the exposure of an RGD-like RYD site. Eur J Cell Bio 1992;58:271–279. [PubMed: 1425765]
64. Alon R, Bayer EA, Wilchek M. Cell adhesion to streptavidin via RGD-dependent integrins. Eur J Cell Bio 1993;60:1–11. [PubMed: 8462588]
65. Escribano J, Hernando N, Ghosh S, Crabb J, Coca-Prados M. cDNA from human ocular ciliary epithelium homologous to βig-h3 is preferentially expressed as an extracellular protein in the corneal epithelium. J Cell Phys 1994;160:511–521.

66. Hirano K, Klintworth GK, Zhan Q, Bennett K, Cintron C. βig-h3 is synthesized by corneal epithelium and perhaps endothelium in Fuchs' dystrophic corneas. Curr Eye Res 1996;15:965–972. [PubMed: 8921218]
67. Ferguson JW, Mikesh MF, Wheeler EF, et al. Developmental expression patterns of Beta-ig (betaIG-H3) and its function as a cell adhesion protein. Mech Dev 2003a;120:851–64. [PubMed: 12963107]
68. Billings PC, Whitbeck JC, Adams CS, et al. The transforming growth factor-β-inducible matrix protein βig-h3 interacts with fibronectin. J Biol Chem 2002;277:28003–28009. [PubMed: 12034705]
69. Kim MO, Yun SJ, Kim IS, Sohn S, Lee EH. Transforming growth factor-beta-inducible gene-h3 (beta (ig)-h3) promotes cell adhesion of human astrocytoma cells in vitro: implication of alpha6beta4 integrin. Neurosci Lett 2003;336:93–6. [PubMed: 12499048]
70. Ferguson JW, Thoma BS, Mikesh MF, et al. The extracellular matrix protein betaIG-H3 is expressed at myotendinous junctions and supports muscle cell adhesion. Cell Tissue Res 2003b;313:93–105. [PubMed: 12838408]
71. Lee SH, Bae JS, Park SH, et al. Expression of TGF-β-induced matrix protein βig-h3 is up-regulated in the diabetic rat kidney and human proximal tubular epithelial cells treated with high glucose. Kidney International 2003;64:1012–1021. [PubMed: 12911551]
72. Oh JE, Kook JK, Min BM. Big-h3 induces keratinocyte differentiation via modulation of involucrin and transglutaminase expression through the integrin α3β1 and the phosphatidylinositol 3-kinase/Akt signaling pathway. J Biol Chem 2005;280:21629–21637. [PubMed: 15805105]
73. Tang J, Wu YM, Zhao P, Jiang JL, Chen ZN. {beta}ig-h3 interacts with {alpha}3{beta}1 integrin to promote adhesion and migration of human hepatoma Cells. Exp Biol Med (Maywood) 2009;234:35–39. [PubMed: 18997105]
74. Park SH, Choi SY, Kim MH, et al. The TGF-β-induced gene product, βig-h3: its biological implications in peritoneal dialysis. Nephrol Dial Transplant 2008;23:126–35. [PubMed: 17704110]
75. Becker J, Erdlenbruch B, Noskova I, et al. Keratoepithelin suppresses the progression of experimental human neuroblastomas. Cancer Res 2006;66:5314–5321. [PubMed: 16707457]
76. Lee BH, Bae JS, Park RW, Kim JE, Park JY, Kim IS. betaig-h3 triggers signaling pathways mediating adhesion and migration of vascular smooth muscle cells through alphavbeta5 integrin. Exp Mol Med 2006;38:153–61. [PubMed: 16672769]
77. Midwood KS, Mao Y, Hsia HC, Valenick LV, Schwarzbauer JE. Modulation of cell-fibronectin matrix interactions during tissue repair. J Investig Dermatol Symp Proc 2006;11:73–8.
78. Said N, Najwer I, Motamed K. Secreted protein acidic and rich in cysteine (SPARC) inhibits integrin-mediated adhesion and growth factor-dependent survival signaling in ovarian cancer. Am J Pathol 2007;170:1054–63. [PubMed: 17322388]
79. Ohno S, Doi T, Tsutsumi S, et al. RGD-CAP ((beta)ig-h3) is expressed in precartilage condensation and in prehypertrophic chondrocytes during cartilage development. Biochim Biophys Acta 2002;1572:114–22. [PubMed: 12204340]
80. Park SW, Bae JS, Kim KS, et al. Beta ig-h3 promotes renal proximal tubular epithelial cell adhesion, migration and proliferation through the interaction with alpha3beta1 integrin. Exp Mol Med 2004;36:211–9. [PubMed: 15272232]
81. Weinreb PH, Simon KJ, Rayhorn P, et al. Function-blocking integrin alphavbeta6 monoclonal antibodies: distinct ligand-mimetic and nonligand-mimetic classes. J Biol Chem 2004;279:17875–87. [PubMed: 14960589]
82. Ohno S, Noshiro M, Makihira S, et al. RGD-CAP (βig-h3) enhances the spreading of chondrocytes and fibroblasts via integrin α1β1. Biochimica et Biophysica Acta 1999;1451:196–205. [PubMed: 10446401]
83. Kim JE, Kim SJ, Lee BH, Park RW, Kim KS, Kim IS. Identification of motifs for cell adhesion within the repeated domains of transforming growth factor-beta-induced gene, betaig-h3. J Biol Chem 2000;275:30907–15. [PubMed: 10906123]
84. Bae JS, Lee SH, Kim JE, et al. Betaig-h3 supports keratinocyte adhesion, migration, and proliferation through alpha3beta1 integrin. Biochem Biophys Res Commun 2002;294:940–8. [PubMed: 12074567]

85. Kim JE, Jeong HW, Nam JO, et al. Identification of motifs in the fasciclin domains of the transforming growth factor-beta-induced matrix protein betaig-h3 that interact with the alphavbeta5 integrin. J Biol Chem 2002a;277:46159–65. [PubMed: 12270930]

86. McBrien NA, Metlapally R, Jobling AI, Gentle A. Expression of collagen-binding integrin receptors in the mammalian sclera and their regulation during the development of myopia. Invest Ophthalmol Vis Sci 2006;47:4674–82. [PubMed: 17065473]

87. Metlapally R, Jobling AI, Gentle A, McBrien NA. Characterization of the integrin receptor subunit profile in the mammalian sclera. Mol Vis 2006;12:725–34. [PubMed: 16862067]

88. Lightner VA, Erickson HP. Binding of hexabrachion (tenascin) to the extracellular matrix and substratum and its effect on cell adhesion. J Cell Sci 1990;9:263–77. [PubMed: 1695220]

89. Murphy-Ullrich JE, Mosher DF. Interactions of thrombospondin with cells in culture: rapid degradation of both soluble and matrix thrombospondin. Semin Thromb Hemost 1987;13:343–51. [PubMed: 3317841]

90. Lahav J. Thrombospondin inhibits adhesion of endothelial cells. Exp Cell Res 1988;177:199–204. [PubMed: 3391237]

91. Murphy-Ullrich JE, Höök M. Thrombospondin modulates focal adhesions in endothelial cells. J Cell Biol 1989;109:1309–19. [PubMed: 2768342]

92. McBrien NA, Young TL, Pang CP, et al. Myopia: Recent Advances in Molecular Studies; Prevalence, Progression and Risk Factors; Emmetropization; Therapies; Optical Links; Peripheral Refraction; Sclera and Ocular Growth; Signalling Cascades; and Animal Models. Optom Vis Sci 2009;86:45–66.

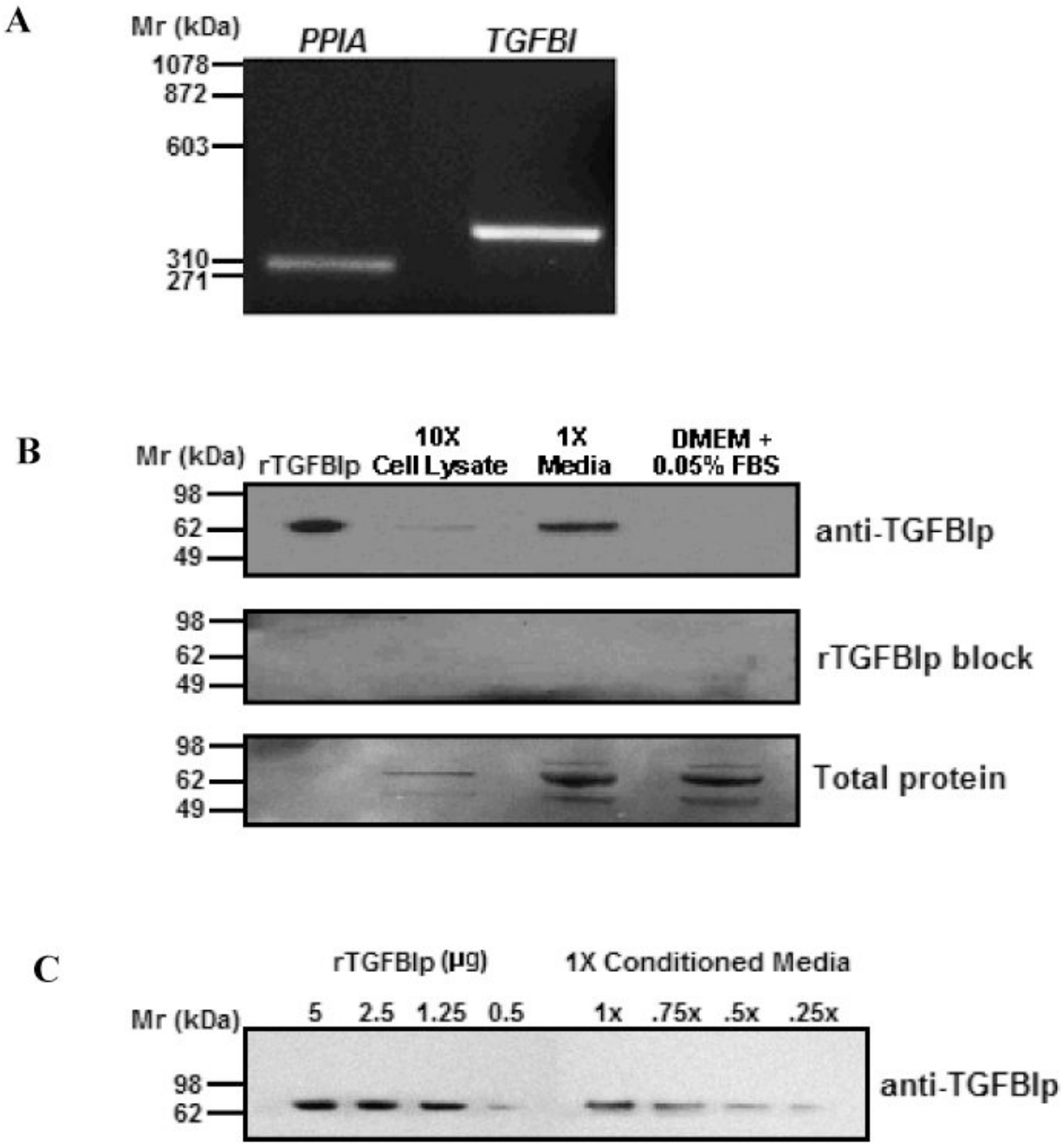

Figure 1. ***TGFBI*/TGFBIp expression in 48 hr serum-starved HSFs**

A) RT-PCR amplification of *TGFBI* (373 bp) and cyclophilin (*PPIA*, 300 bp) from HSFs. **B)** Western blot of HSF cell lysates (10×) and media (1×) probed with anti-TGFBIp (top panel). Human recombinant TGFBIp (rTGFBIp, 40 ng) and DMEM containing 0.05% FBS served as the positive and negative control, respectively. Pre-incubation of anti-TGFBIp with an equimolar amount of rTGFBIp (1μM) for 1 hr at room temperature abolished all immunopositive bands, confirming the specificity of the antibody (rTGFBIp block, middle panel). Total protein loaded in each lane was visualized by Coomasie blue (bottom panel). **C)** The indicated quantities of rTGFBIp were compared with several dilutions of 48 hr HSF conditioned medium (10 μl/lane).

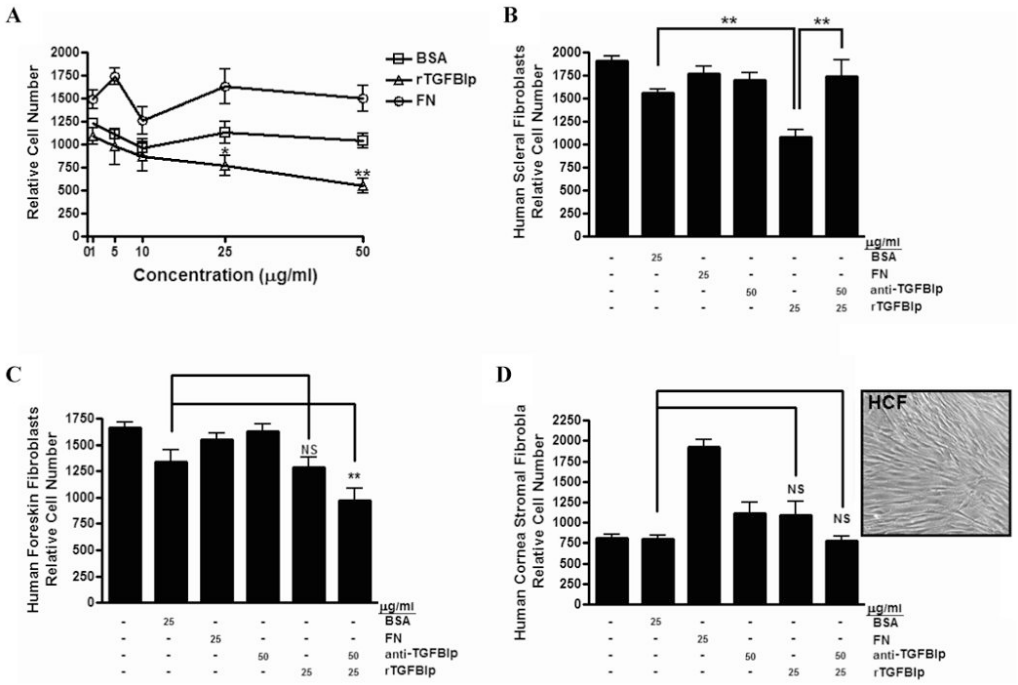

Figure 2. Inhibitory role of TGFBIp on cell attachment is specific to HSFs

A) HSF attachment to collagen type I in the presence of BSA, FN, or rTGFBIp (1 – 50 μg/ml). **B)** HSF attachment to collagen type I in the presence of BSA, FN, rTGFBIp (25 μg/ml) with or without anti-TGFBIp (50 μg/ml). **C)** Attachment of HFFs to collagen type I in the presence of BSA, FN, rTGFBIp (25 μg/ml) with or without anti-TGFBIp (50 μg/ml). **D)** Attachment of HCFs to collagen type I in the presence of BSA, FN, rTGFBIp (25 μg/ml) with or without anti-TGFBIp (50 μg/ml). Micrograph of HCFs prior to harvesting for cell attachment assays demonstrating a distinct fibroblast phenotype (inset). NS, not significant; BSA, bovine serum albumin; FN, fibronectin. Data are expressed as the mean ± SEM by the Student's *t*-test for unmatched pairs for three individual experiments in triplicate (*$p < 0.05$ and **$p < 0.01$).

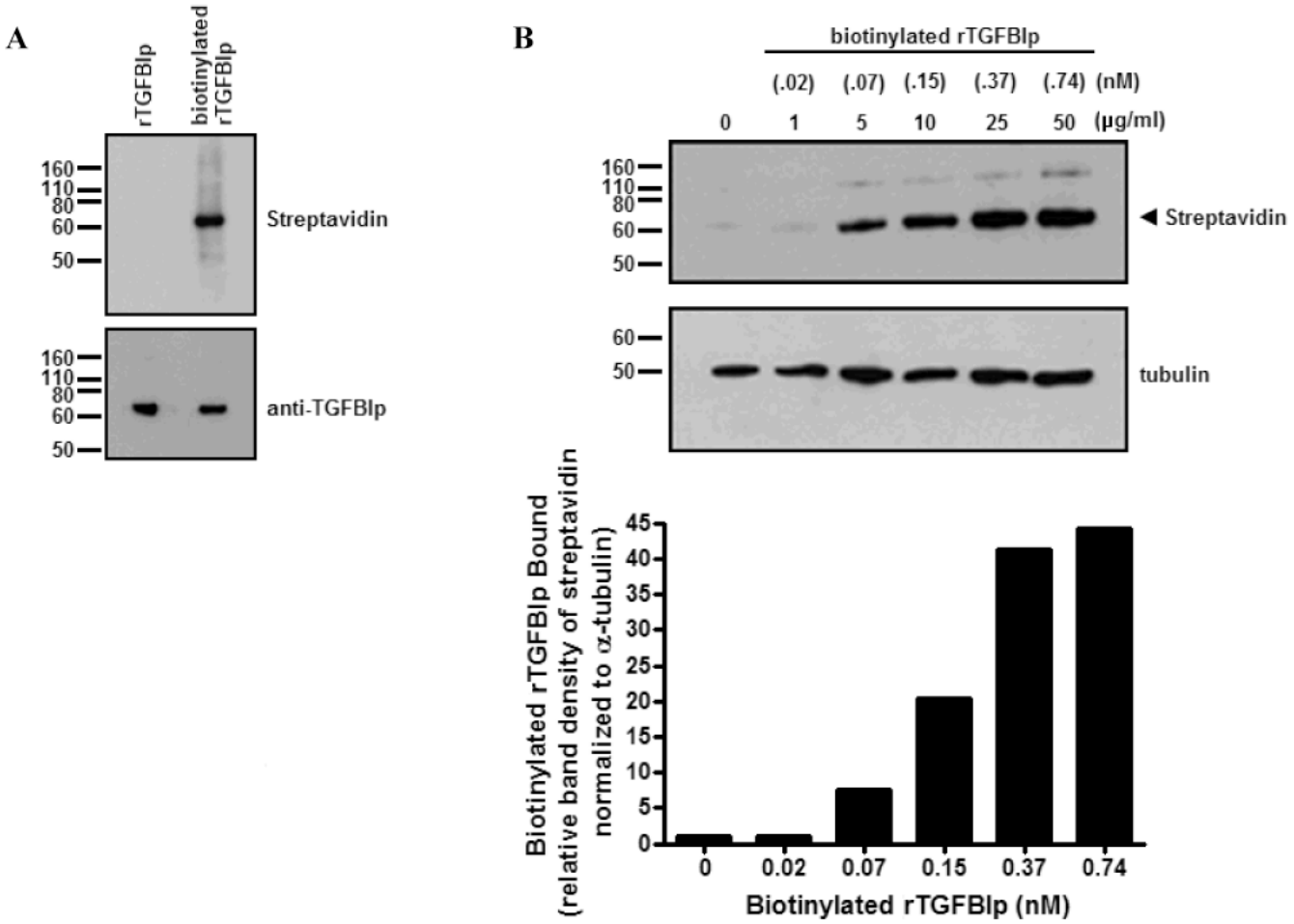

Figure 3. TGFBIp binds to the surface of HSFs in a dose dependent manner

A) Western blot of both rTGFBIp (100 ng) and biotinylated rTGFBIp (100 ng). Blots were probed with streptavidin conjugated to alkaline phosphatase, then stripped and reprobed with anti-TGFBIp. **B)** Western blot of HSF lysates incubated with increasing concentrations of biotinylated rTGFBIp (0 – 50 µg/ml) probed with streptavidin conjugated to alkaline phosphatase, and band densities quantified in the histogram (below). Binding of biotinylated rTGFBIp to HSFs was saturable at ≥ 0.37 nM (25 µg/ml; Bmax).

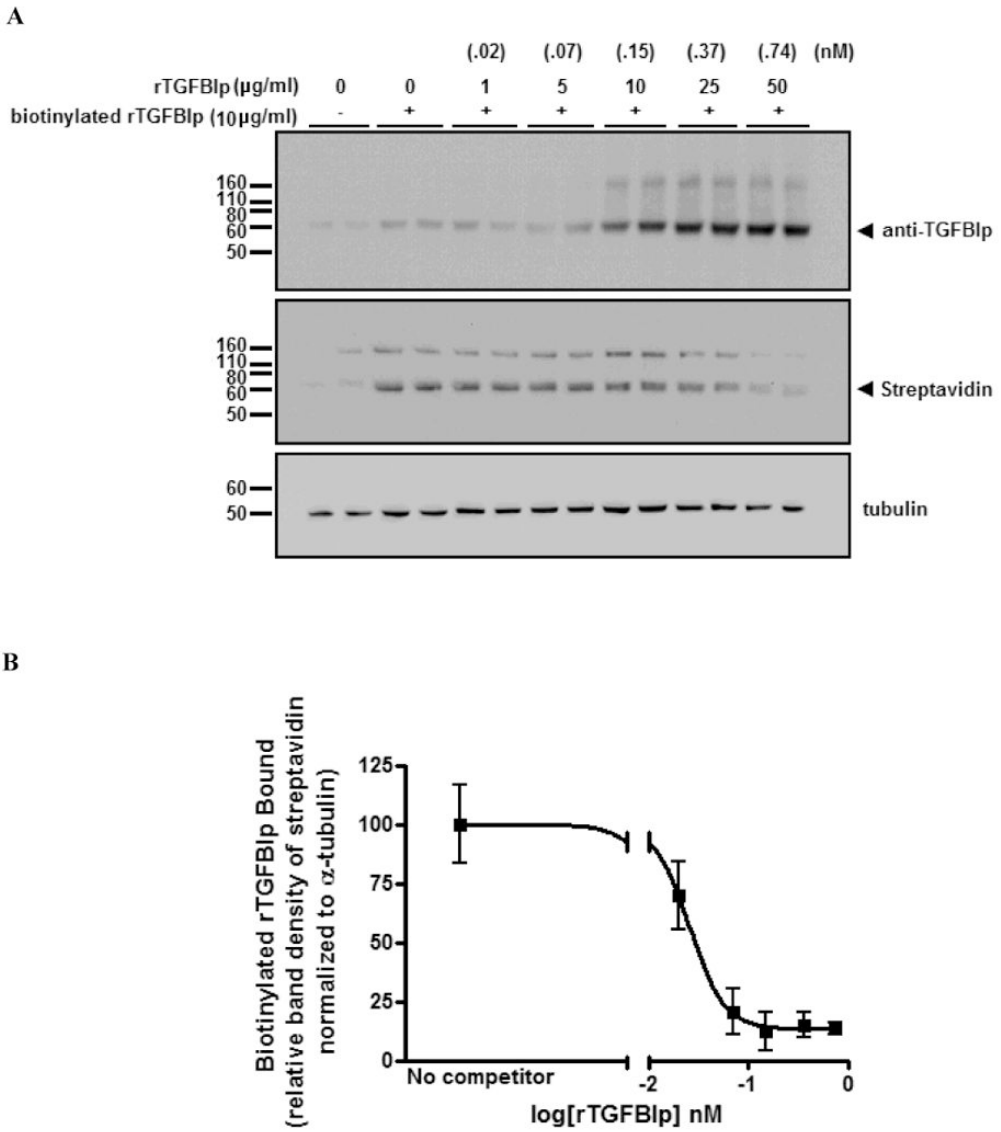

Figure 4. Competition binding assay

A) Representative western blot from three independent experiments in duplicate of cell lysates from HSFs incubated with soluble biotinylated rTGFBIp in the presence of increasing amounts of nonbiotinylated rTGFBIp (competitor) probed with anti-TGFBIp and streptavidin conjugated to alkaline phosphatase. Note reduced biotinylated rTGFBIp binding in the presence of competitor. **B)** Competitive inhibition curve for specific binding of biotinylated rTGFBIp by increasing concentrations of nonbiotinylated rTGFBIp. The 50% inhibition concentration ($\log IC_{50}$) was calculated to be -1.54 nM (IC_{50} = .03 nM). Data is expressed as band intensity of biotinylated rTGFBIp relative to α-tubulin. The data were fitted into an IC_{50} equation using GraphPad Prism software. For the loading control, all blots were stripped and reprobed with α-tubulin antibody. Arrowhead indicates position of the 68 kD band.

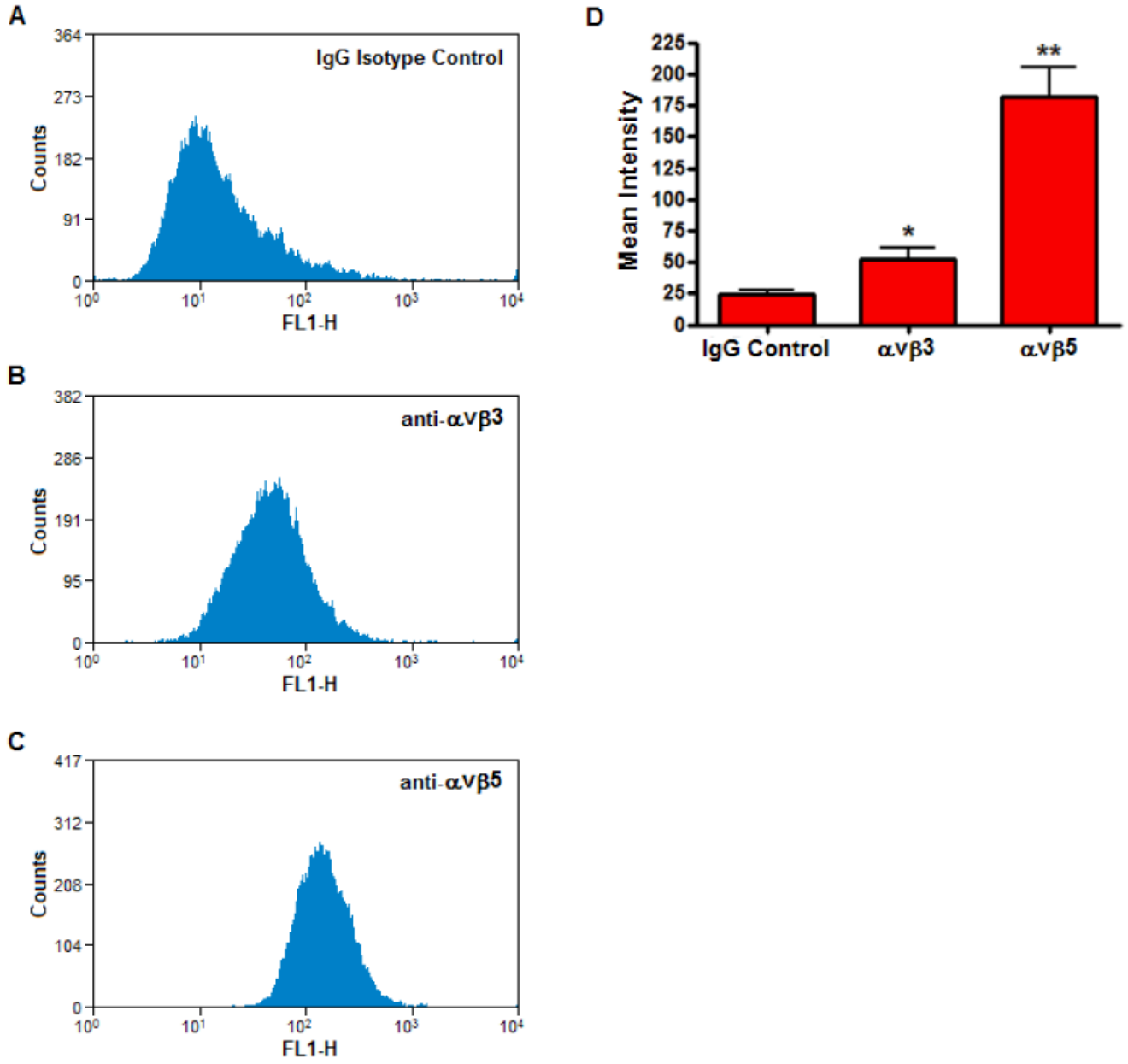

Figure 5. Integrin expression on the surface of HSFs

Flow cytometry on live HSFs incubated with 4 μg/ml of IgG isotype control **(A)**, or the monoclonal antibodies, anti-αvβ3 **(B)** and anti-αvβ5 **(C)**. The data are expressed as cell counts (*y*-axis) plotted as a function of fluorescence intensity (*x*-axis) and are representative of three independent experiments. **D)** Histogram represents the mean intensities of anti-αvβ3 and anti-αvβ5 from flow cytometric analysis as compared to the IgG isotype control. Data are expressed as the mean ± SEM by the Student's *t*-test for unmatched pairs for four individual experiments (*$p < 0.05$, **$p < 0.01$).

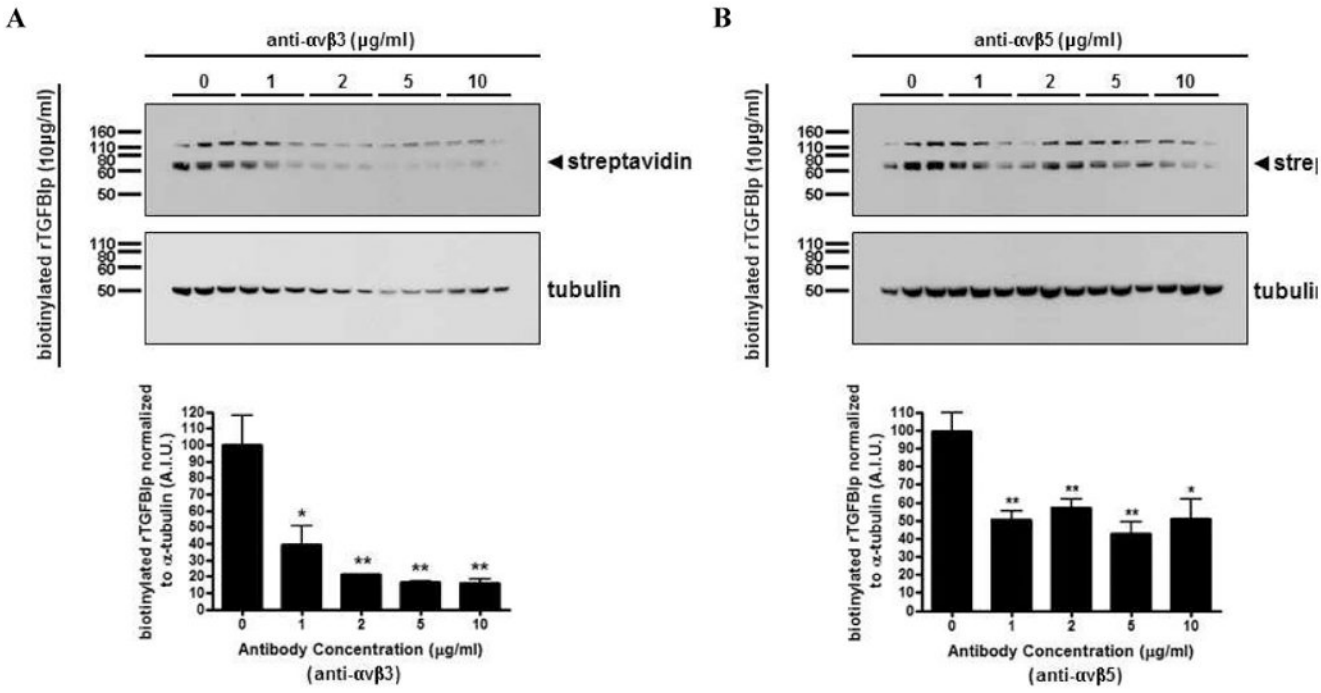

Figure 6. TGFBIp binds to HSFs by interacting with αvβ3 and αvβ5 integrins

Western blot of cell lysates collected from HSFs preincubated with the function-blocking monoclonal antibodies (0 – 10 μg/ml) against αvβ3 **(A)** and αvβ5 **(B)** for 1 hr at 4 °C, before the addition of biotinylated rTGFBIp (10 μg/ml) for 5 hr at 4 °C. Blots were probed with streptavidin conjugated to alkaline phosphatase (upper panels), stripped and reprobed with α-tubulin antibody (lower panels). Arrowhead represents the biotinylated rTGFBIp (~68 kD). Histograms represent the relative band intensities quantified, and each band was normalized to their corresponding α-tubulin. Data are expressed as the mean ± SEM by the Student's *t*-test for unmatched pairs for three individual experiments in triplicate (*$p < 0.05$, **$p < 0.01$).

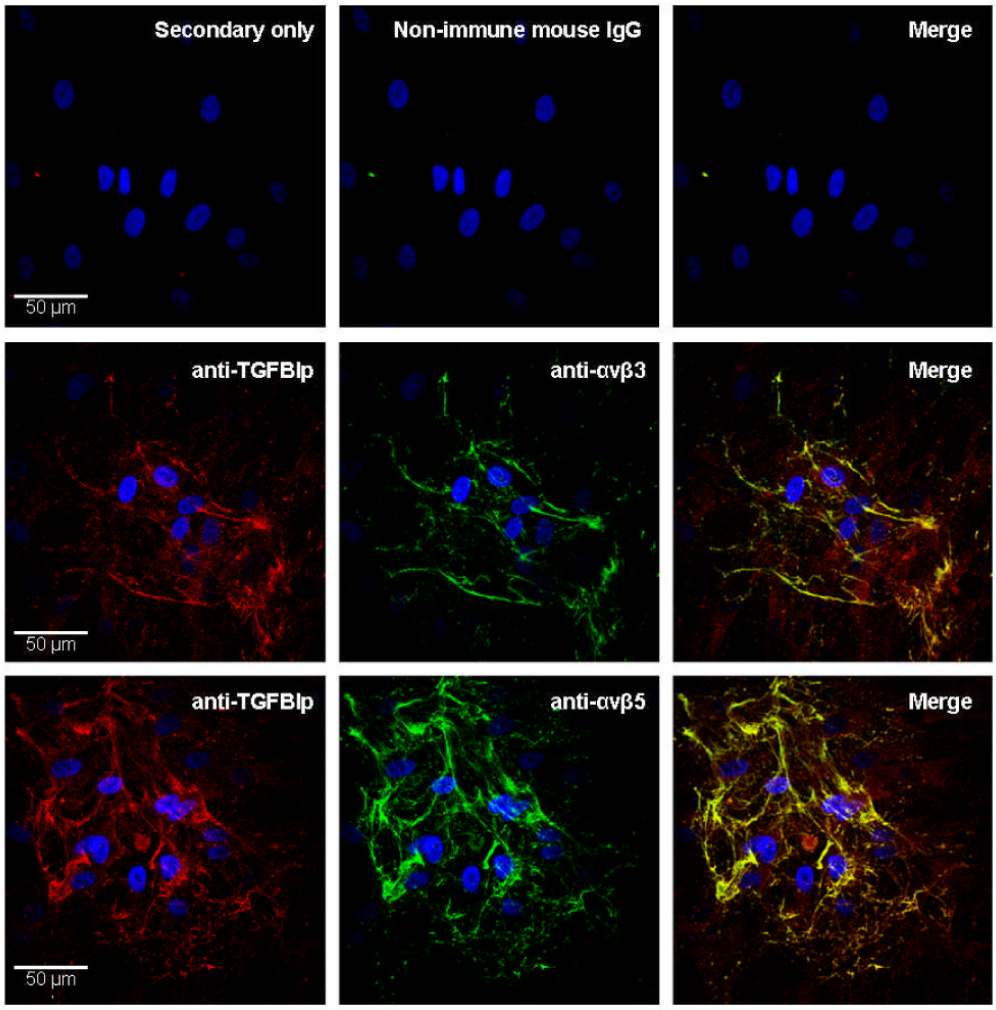

Figure 7. Colocalization of TGFBIp to αvβ3 and αvβ5 integrins in HSFs

Immunofluorescence of TGFBIp (red) on the surface of HSFs double labeled either with anti-αvβ3 (green; top), or with anti-αvβ5 (green, bottom). The right panels are the merged images and areas of colocalization are indicated by yellow. The nuclei are counterstained with DAPI (blue). No signal was detected in secondary antibody only or non-immune mouse IgG controls.